

Article

Phospholipid-Based Topical Nano-Hydrogel of Mangiferin: Enhanced Topical Delivery and Improved Dermatokinetics

Faisal K. Alkholifi ¹ , Aftab Alam ^{2,*} , Ahmed I. Foudah ²  and Hasan S. Yusufoglu ³ 

¹ Department of Pharmacology, College of Pharmacy, Prince Sattam Bin Abdulaziz University, Al Kharj 11942, Saudi Arabia

² Department of Pharmacognosy, College of Pharmacy, Prince Sattam Bin Abdulaziz University, Al Kharj 11942, Saudi Arabia

³ Department of Pharmacognosy & Pharmaceutical Chemistry, College of Dentistry & Pharmacy, Buraydah Private Colleges, Buraydah 51418, Saudi Arabia

* Correspondence: a.alam@psau.edu.sa

Abstract: Mangiferin is a herbal drug that has proven anticancer potential. Owing to its lower aqueous solubility and poor oral bioavailability, the full pharmacological potential of this bioactive drug has not fully been explored. In the present study, phospholipid-based microemulsion systems were developed to bypass oral delivery. The globule size of the developed nanocarriers was less than 150 nm and the drug entrapment was >75% with a drug loading ~25%. The developed system offered a controlled release pattern following the Fickian drug release. This enhanced mangiferin's in vitro anticancer activity by four-fold, the cellular uptake was observed to be improved by three-fold on the MCF-7 cells. Ex vivo dermatokinetic studies showed substantial topical bioavailability with a prolonged residence time. The findings provide a simple technique to administer mangiferin via a topical route promising a safer, topically bioavailable and effective treatment option for breast cancer. Such scalable carriers with immense topical delivery potential may provide a better option for present-day topical products of a conventional nature.

Keywords: dermal bioavailability; dermal pharmacokinetics; topical administration; nanoemulsion; microemulsion; anticancer; breast cancer



Citation: Alkholifi, F.K.; Alam, A.; Foudah, A.I.; Yusufoglu, H.S. Phospholipid-Based Topical Nano-Hydrogel of Mangiferin: Enhanced Topical Delivery and Improved Dermatokinetics. *Gels* **2023**, *9*, 178. <https://doi.org/10.3390/gels9030178>

Academic Editors: Lan Xiao, Chun Xu and Wendong Gao

Received: 19 January 2023

Revised: 17 February 2023

Accepted: 20 February 2023

Published: 24 February 2023



Copyright: © 2023 by the authors. Licensee MDPI, Basel, Switzerland. This article is an open access article distributed under the terms and conditions of the Creative Commons Attribution (CC BY) license (<https://creativecommons.org/licenses/by/4.0/>).

1. Introduction

Mangiferin, chemically known as 2-β-D-glucopyranosyl-1,3,6,7-tetrahydroxy-9H-xanthen-9-one, is extracted from the seed, peel and kernel of *Mangifera indica* and other plants of higher order. This plant possesses immense potential for managing breast cancer, as reported in the literature. Recent scientific studies have established the beneficial effects of mangiferin, not only limited to immunomodulation, lipid-lowering, anticancer, antioxidant, antidiabetic, antiallergic and antimicrobial effects, but have been further reported for many lifestyle-related disorders [1–3]. The anticancer potential of this bioactive molecule has been explored by researchers all over the globe for benefits in breast, colon, lung and neuronal cancers. This phytoconstituent acts by various mechanisms ranging from free radical scavenging to the induction of apoptosis [4]. It is an acceptable trend that phytochemicals are explored for multiple therapeutic benefits [5,6], but numerous challenges are associated with the delivery of phytochemicals [7,8].

Like most phytochemicals, mangiferin is associated with problems such as higher lipophilicity, lesser solubility in biological fluids and poor bioavailability [9]. The oral bioavailability of mangiferin is reported to be lower than 2% [10]. Numerous reports are available where emulsifying systems have enhanced the bioavailability of poorly bioavailable drugs [11]. Drug delivery carriers such as adhesive nanocarriers [12], PEGylated carbon nanotubes [10], injectable hydrogels [13], nano-mixed micelles [14] and nanostruc-

tured lipid carriers [15] have been developed by researchers to deliver this promising drug by one route or another.

Since oral delivery represents a challenge, it was envisioned that topical formulations were developed employing the principles of drug delivery and biocompatible components such as phospholipids [16]. Phospholipids, made of biocompatible material and an integral part of biological membranes, were selected as an important component for developing microemulsion-based gel [17]. Microemulsion systems are known to properly dissolve and deliver the drug across the skin barriers [18]. Therefore, it was envisioned to explore the effect of phospholipid-incorporated microemulsion-based topical gel on the topical bioavailability of this promising phytochemical and provide a proof-of-concept to the scientific fraternity along with the possible biological evaluations. However, researchers have utilised microemulsions for topical delivery [18,19], but for mangiferin, no such topical product has been explored for the anticancer potential. A few attempts have been made to develop the nanoemulsions of this bioactive and explore its potential in inflammation and skin regeneration. The materials, process and approach of the previously published literature are different from the present research, vouching for the novelty of the current work [20].

2. Results and Discussion

2.1. Construction of Pseudo-Ternary Phase Diagrams

A total of three pseudo-ternary phase diagrams were constructed. Isopropyl palmitate (IPP) was used as the oil and Gelucire 44/14 and Labrasol were used as the surfactant and cosurfactants in S_{mix} ratios of 1:1, 2:1 and 3:1, respectively. Figures 1–3 show the pseudoternary phase diagrams prepared with IPP, water and S_{mix} ratios of 1:1, 2:1 and 3:1, respectively.

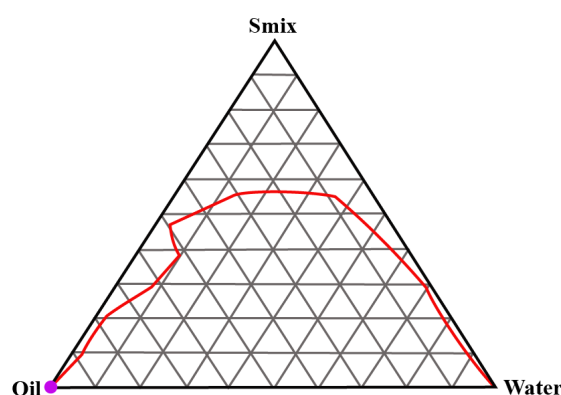


Figure 1. Pseudoternary phase diagram between IPP, water and S_{mix} (1:1). The red line shows the boundary between the monophasic and biphasic region. The area above redline represents the monophasic region.

The monophasic area obtained in all three ternary phase diagrams was relatively wider in range. It invariably increased with the increase in the surfactant-to-cosurfactant ratio. Labrasol, a polyethylene glycol derivative of capric acid and caprylic acid triglycerides, offers excellent emulsification properties for various oils. Gelucire 44/14 is composed of polyoxylglycerides with well-established emulsification attributes [21,22]. From these pseudoternary phase diagrams, a total of 9 formulations were selected and preceded further.

2.2. Optimisation of the Microemulsion Composition

The nine selected formulations were characterised for particle size, drug entrapment (% EE) and drug loading (% DL). The details of the obtained results are presented in Table 1.

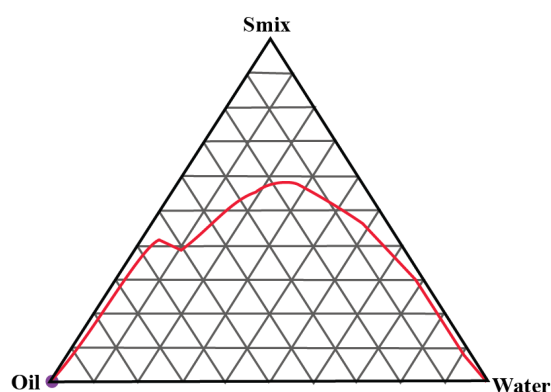


Figure 2. Pseudoternary phase diagram between IPP, water and S_{mix} (2:1). The red line shows the boundary between the monophasic and biphasic region. The area above redline represents the monophasic region.

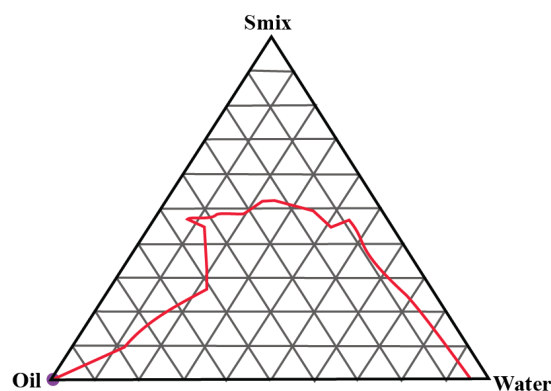


Figure 3. Pseudoternary phase diagram between IPP, water and S_{mix} (3:1). The red line shows the boundary between the monophasic and biphasic region. The area above redline represents the monophasic region.

Table 1. The characterisation of various developed microemulsion formulations.

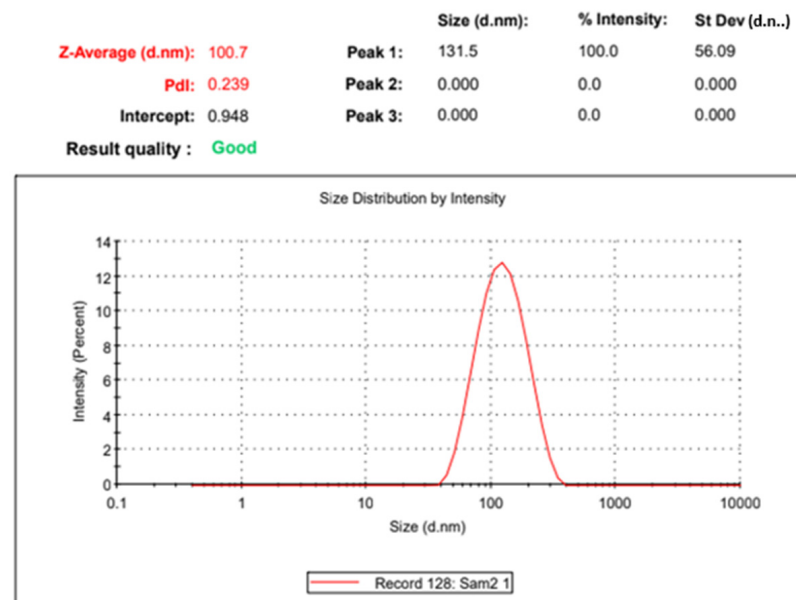
Code	F1	F2	F3	F4	F5	F6	F7	F8	F9
Size (nm)	286.59	254.35	278.20	185.73	179.34	210.62	118.55	100.7	114.91
% EE	78.29	82.33	82.17	76.87	81.75	79.94	76.09	83.43	82.18
% DL	11.74	12.41	12.32	11.53	12.26	11.99	11.41	12.51	12.32

The globule size of the selected formulations was below 300 nm and invariably for every oil composition; it was least for the 2:1 surfactant-to-cosurfactant ratio with the least value for the formulation F8. The 2:1 S_{mix} ratio offered better emulsification to all the oil compositions resulting in a smaller globule size. The total formulation-to-drug ratio was of approximately 6.7. Therefore, the entrapment efficiency for each formulation was >75% with the maximum drug entrapment offered by formulation F3. A pattern analogous to the globule size was also observed in drug entrapment. For each oil composition, the drug entrapment was lower at both the 1:1 and 3:1 S_{mix} ratios and the highest at the intermediate ratio of 2:1. For drug loading, a similar pattern was also observed, which was the best for F8 followed by F2. Based on the least globule size and highest entrapment efficiency/drug loading, formulation F8 was selected as the optimised formulation.

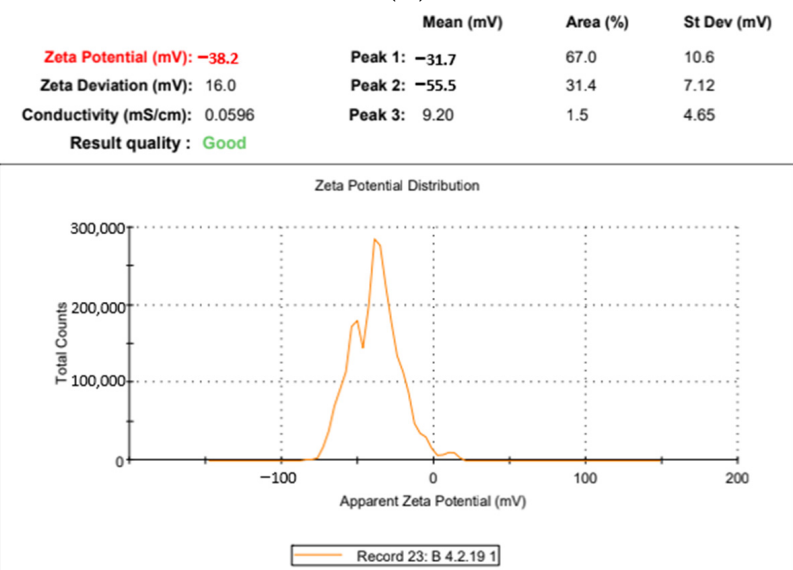
2.3. Polydispersity, pH, Zeta-Potential and Morphology

The globule size of the optimised microemulsion formulation was 100.7 ± 18.7 nm with a PDI value of 0.239. The lower size range of globules assured a nanoemulsion

formulation with a PDI confirming the reliability of the micromeritic data of the dispersed phase. The zeta potential of the developed nanodispersion derived from the F8 formulation was -38.2 ± 7.46 mV, assuring substantial dispersion stability [23,24]. The particle size and zeta potential results are shown in Figure 4A,B, respectively.



(A)



(B)

Figure 4. (A): The globule size, polydispersity index and globule size distribution of the formulation F8. (B): The zeta-potential graph of the formulation F8.

The transmission electron microscopy confirmed the formation of spherical globules devoid of any aggregation, as shown in Figure 5. The pH of the selected formulation was 6.92 ± 0.21 , which is within the range for the topical products that are well tolerated on the skin [25].

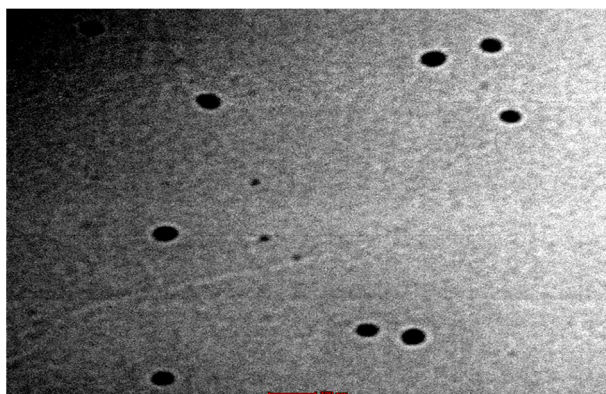


Figure 5. The TEM microphotograph of the microemulsion formulation F8.

2.4. Fourier Transform Infrared Spectroscopy

The results of the FT-IR are shown in Figure 6. Figure 6A represents the FT-IR spectrum of mangiferin with secondary hydroxyl peak at 3374 cm^{-1} ; anti-symmetric C–H stretching at 2941 cm^{-1} ; symmetric C–H stretching at 2890 cm^{-1} ; C=O stretching at 1652 cm^{-1} ; CH–CH bending at 1502 cm^{-1} ; and C–C stretching at 1103 cm^{-1} . The microemulsion (Figure 6B) peaks appeared for the OH- bond at 3429 cm^{-1} , C–H stretch at 2928 cm^{-1} ; C=O stretch at 1739 cm^{-1} ; C=O bending at 1648 cm^{-1} ; C–H bending at 1467 cm^{-1} ; and C–O stretching at 1111 cm^{-1} , indicating no interactions between the drug and the excipients, or even just among the excipients. Figure 6C represents the FT-IR spectra of Labrasol with the characteristic C–H stretch 2904 cm^{-1} ; C=O stretch 1739 cm^{-1} ; C–H bending at 1473 cm^{-1} ; and C–O stretch 1103 cm^{-1} . Figure 6D shows the FT-IR spectrum of the oil with the O–H stretch at 3447 cm^{-1} ; C–H stretching asymmetric 2928 cm^{-1} ; and C–H symmetric 2862 cm^{-1} ; C=O stretch at 1739 cm^{-1} ; and C–O stretching at 1117 cm^{-1} . Figure 6E represents the FT-IR spectra of the Gelucire showing characteristic C–H stretch 2932 cm^{-1} , C=O stretch 1745 cm^{-1} and C–O stretch 1113 cm^{-1} .

2.5. Incorporation in the Hydrogel

The final composition of the nano-hydrogel was 0.02 g of mangiferin/g of the gel, 0.1578 g of oil/g of gel, 0.6316 g of S_{mix} , 0.0125 g of Carbopol, 934/g of gel, 0.0125 g of triethanolamine/g of gel, 0.01 g of phospholipid/g of gel and 0.1556 g of water/g of gel. The conventional hydrogel contained 0.02 g of mangiferin/g of gel, 0.0125 g of Carbopol 934/g of gel, 0.0125 g of triethanolamine/g of gel, 0.0125 g ethanol/g of gel and 0.9425 g of water/g of gel.

2.6. Rheological Studies of the Nano-Hydrogel

The graph between the shear stress and shear rate is shown in Figure 7A. The graph shows the variation in the shear stress as a function of shear rate. It is clear that, with an increase in the shear rate, the shear stress of the system increased. The system offered a non-Newtonian behaviour with a plastic flow and offered a yield value of 50 Pa. The average viscosity of the developed system was 8.7 Pa·s. The studies clearly vouch that the developed system behaved as a Newtonian after the yield value. Such behaviour is desired for the gelled system and is suitable for storage in tubes [26]. The rheological profile of the conventional hydrogel is provided in Figure 7B. The viscosity (8.97 Pa·s) and the yield values (61 Pa) of the conventional gel are higher than that of the developed nano-hydrogel owing to the presence of oil and surfactants in the latter.

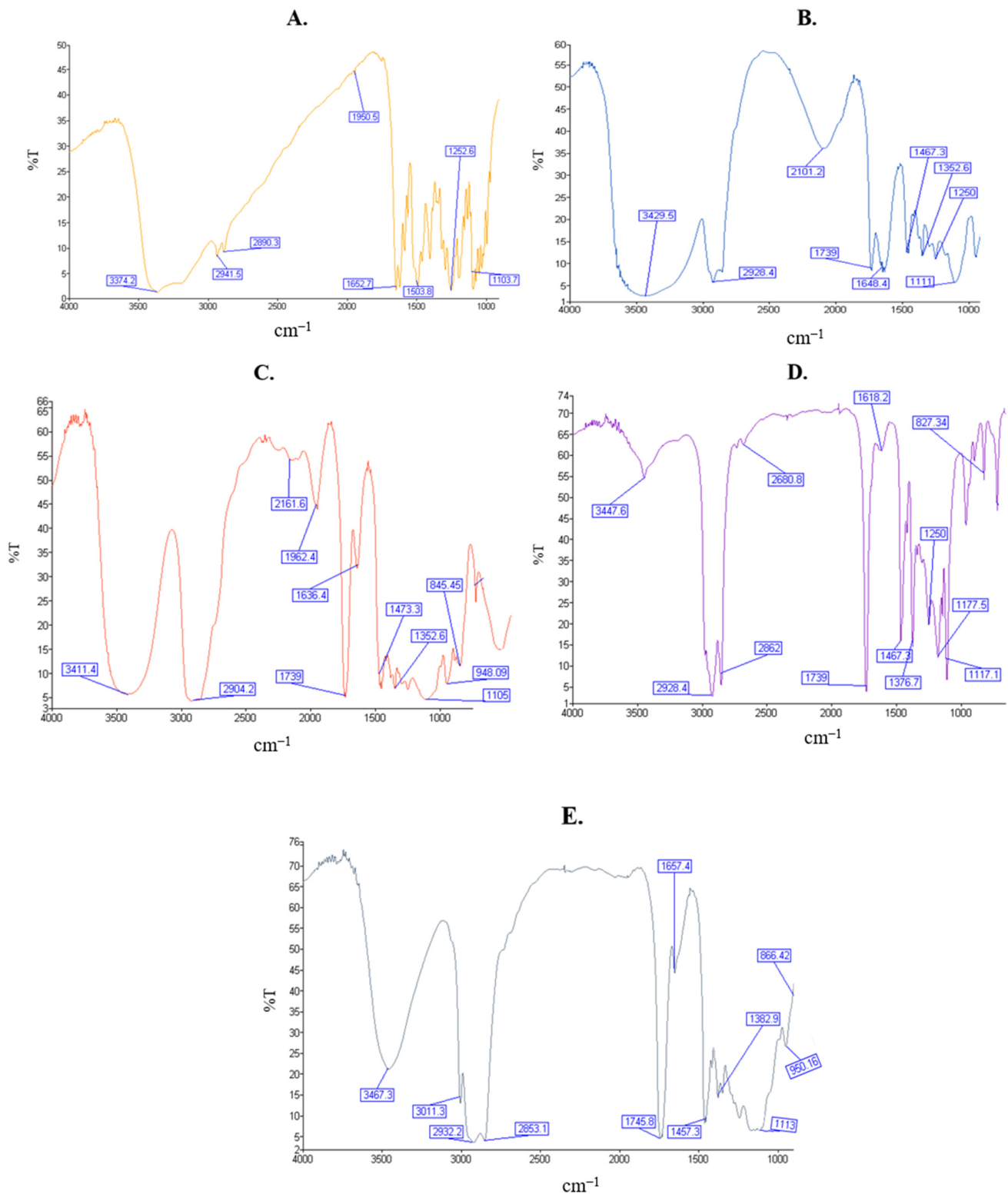


Figure 6. FT-IR spectrum of: mangiferin (A), microemulsion (B), Labrasol (C), IPP (D) and Gelucire (E).

2.7. Drug Permeation and Drug Retention Studies

The drug permeation profile of mangiferin from the optimised microemulsion, nano-hydrogel formulation and the conventional gel for 8 h is shown in Figure 8. From the obtained data, it is clear that the drug permeation from the conventional gel was without any resistance across the skin. In contrast, the drug release was sustained for the nano-

hydrogel formulation. However, the release from the globules of the microemulsion was intermediate. At every time point, there was a significant difference in the release profile from all the systems ($p < 0.05$). The plain drug from the conventional gel was almost completely permeated in 3 h of the study, whereas the nano-hydrogel maintained the drug release for 8 h, advocating a sustained release pattern.

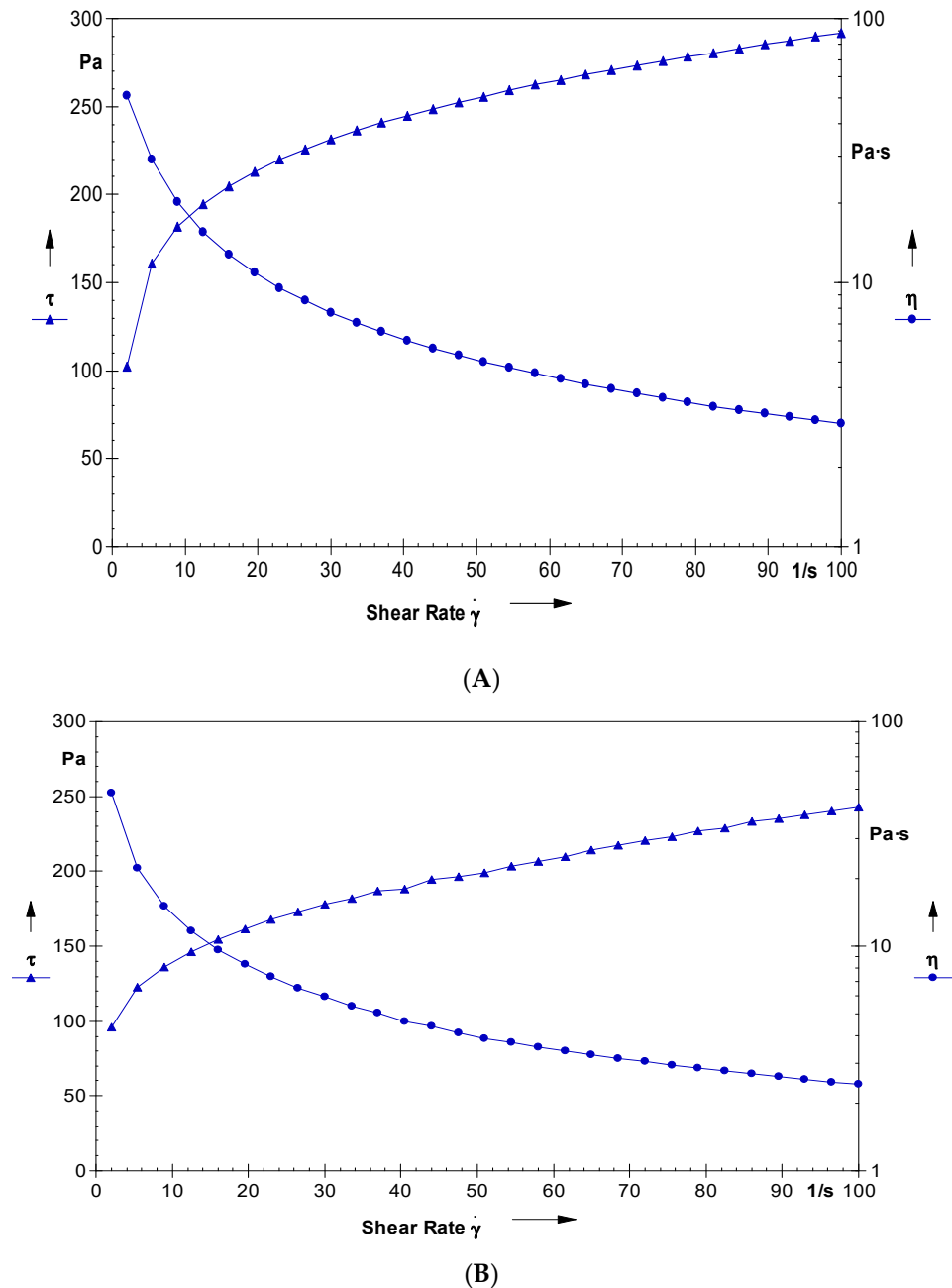


Figure 7. (A): The graph showing the variation in viscosity and shear stress with the varying values of shear rate for the developed nano-hydrogel. (B): The graph showing the variation in viscosity and shear stress with the varying values of shear rate for the developed conventional gel.

On the other hand, the microemulsion could also appreciably control the drug release vis-à-vis the conventional gel. However, the microemulsion's permeation rate was higher than the nano-hydrogel. The average drug permeation rate for the conventional hydrogel was 0.323 mg/h, which was significantly higher than the drug encapsulated in the nano-hydrogel with a permeation rate of 0.116 mg/h ($p < 0.05$). The drug permeation rate for the

microemulsion was 0.139 mg/h, which was significantly higher than the nano-hydrogel and lower than the conventional formulation ($p < 0.05$). The gelling of the nanocarrier resulted in a more controlled release pattern from the microemulsion. The average permeation rate confirmed the controlled release pattern from the nano-hydrogel and drug-loaded microemulsion, whereas the drug permeation mechanism from the plain drug gel was of first order.

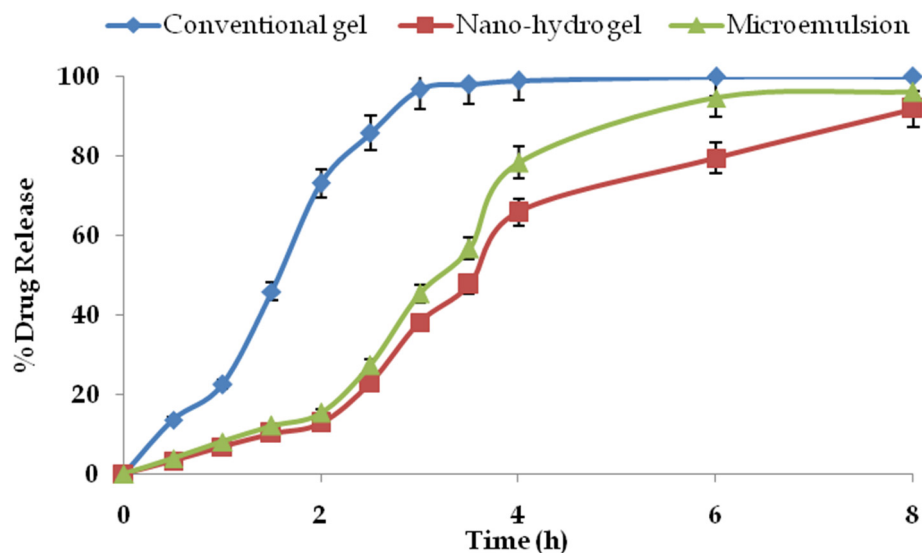


Figure 8. Cumulative drug permeation profiles of mangiferin from the studied systems ($n = 3$).

The drug retention in the skin is shown in Figure 9. The drug retained in the skin for the developed nano-hydrogel was $4.98 \pm 0.02\%$, whereas for the conventional gel, the drug retained in the skin was $0.92 \pm 0.01\%$, whereas the drug retention in the skin from the ungelled microemulsion was $3.07 \pm 0.02\%$. The drug retention in skin layers by the nano-hydrogel was substantially higher than the drug retention by plain gel as well as the ungelled microemulsion, although the values for the microemulsion were significantly higher than the conventional gel ($p < 0.05$). The plausible reasons are the composition and nano-architecture of the microemulsion which resulted in the better adhesion, fusion and depot formation in the skin, which was further facilitated by gelling. Such deposition is desired in topical delivery as the drug will be released from the depot and assured drug concentrations for longer duration [18,27].

2.8. Cancer Cell Viability

MTT-based cell cytotoxicity assay was performed on MCF-7 cells. The IC₅₀ values for the plain mangiferin gel (conventional gel) and the nano-hydrogel-incorporated mangiferin were obtained to be $12.5 \mu\text{g/mL}$ and $6.25 \mu\text{g/mL}$, respectively. On the other hand, the plain gel formulation was found to exhibit no significant toxicity, even at the concentrations above $200 \mu\text{g/mL}$. Interestingly, the IC₅₀ value of the ungelled microemulsion was found to be of the lowest magnitude, i.e., $5.98 \mu\text{g/mL}$. The results are shown in Figure 10. The IC₅₀ values obtained for the drug were in consonance with the previously published results [28]. The substantial decrease in the IC₅₀ value of mangiferin after the encapsulation in microemulsion gel exhibited 100% enhancement in the anticancer activity due to the easy penetration and better availability of drugs as a result of components such as IPP, Gelucire and Labrasol [19,22]. However, the ungelled microemulsion had better cytotoxicity than the nano-hydrogel in the in vitro cytotoxicity assays. This was because the ungelled microemulsion was a low-viscosity liquid that could easily get inside the cancer cells; consequently, the cells were more exposed to the microemulsion.

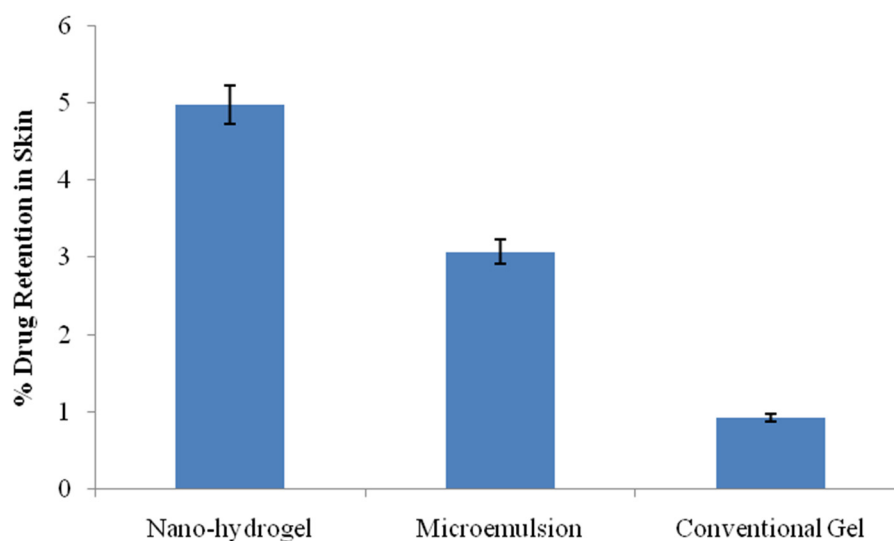


Figure 9. Drug retention in the skin from the studied formulations (n = 3).

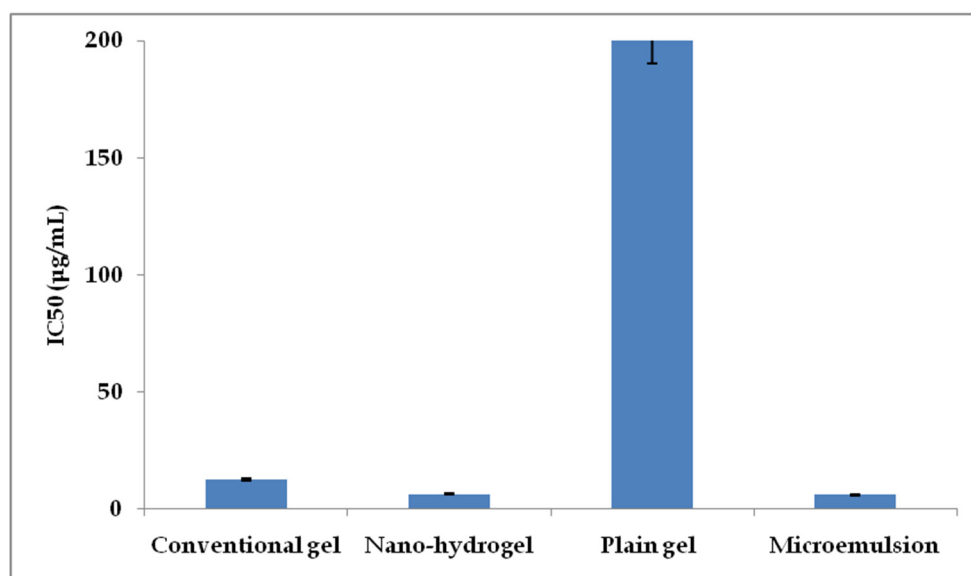


Figure 10. IC₅₀ values of the tested formulations against MCF-7 cell lines.

2.9. Dermatokinetic Studies

The results obtained from the dermal pharmacokinetic studies are shown in Figure 11 and Table 2. As shown in the figure, the drug concentration offered by the nano-hydrogel formulation in skin was substantially higher than the drug concentration from the plain drug gel at every time point ($p < 0.05$). As a poorly absorbed drug, the substantially higher drug concentrations in rodents skin from the nano-hydrogel is a significant achievement [29]. The drug-loaded microemulsion was not the final product for topical application, and the ungelled microemulsion was also studied for comparison. The performance of the microemulsion was slightly better than its gelled version, owing to the apparent reason for diffusion limitation in the gelled system. However, for better retention, the in vivo gels are better. There was 2.5-fold enhancement in the C_{max} and an approximately eight-fold improvement in the area under the curve (AUC). The studies clearly demonstrated the enhanced dermal bioavailability potential of a promising drug using biocompatible components such as IPP, Gelucire and Labrasol. The microemulsion-based nano-hydrogel not only improved the topical bioavailability of the drug, but also improved the half-life and bioresidence of the drug molecule in the dermal/epidermal compartments.

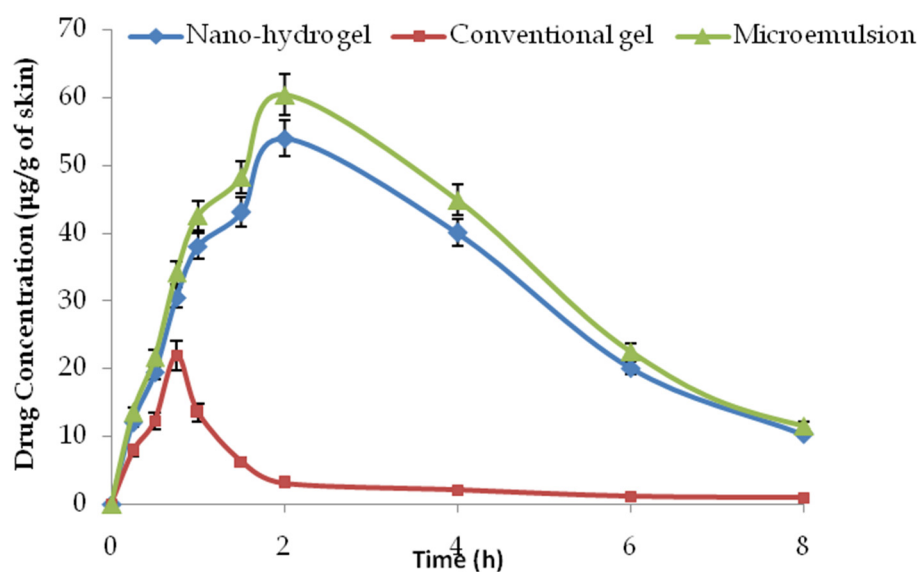


Figure 11. Mean plasma mangiferin concentration versus time graph in rodents (n = 4).

Table 2. The dermal pharmacokinetic parameters obtained from the skin drug concentration–time profile of mangiferin in rodent skin.

Dermatokinetic Parameter	Conventional Gel	Microemulsion	Nano-Hydrogel
C_{max} (µg/g of skin)	21.97 ± 1.98	60.45 ± 4.11	53.98 ± 5.07
T_{max} (h)	0.75	2	2
AUC_0^∞ (µg·mL ⁻¹ ·h)	41.55 ± 9.03	361.31 ± 36.13	328.46 ± 23.18
K_p (h ⁻¹)	1.91	5.01	4.67
K (h ⁻¹)	0.43	0.28	0.29
$T_{1/2}$ (h ⁻¹)	1.61	2.48	2.38

3. Conclusions

The developed microemulsion-based nano-hydrogel formulation with sub-micron size and acceptable zeta-potential not only improved the anticancer activity of mangiferin by two-fold, but also improved the topical bioavailability of this promising bioactive many times. Though the drug was not yet explored in the developed system for topical delivery, the present study provides an option to deliver the drug by topical route with inherent promises such as enhanced permeation, retention, conducive dermal pharmacokinetic profile and improved anticancer potential. Such scalable products using simple preparatory techniques with substantial beneficial outcomes for safety, efficacy and dermal pharmacokinetics provide a ray of hope for the further exploration of such products for better outcomes. A significant understanding of the underlying principles of dermatokinetics, as in this case, can result in the better location of the drug. It can assist in achieving the targets of targeted delivery.

4. Materials and Methods

4.1. Materials

Mangiferin and 3-(4,5-dimethylthiazol-2-yl)-2,5-diphenyltetrazolium bromide (MTT) were purchased from Sigma-Aldrich, St. Louis, MO, USA. The hydrochloric acid, chloroform, isopropyl palmitate (IPP) and methanol was obtained from SDFCL Chem. Limited, India, whereas the buffer reagents, i.e., disodium hydrogen phosphate, sodium chloride and potassium dihydrogen phosphate were supplied by CDH Pvt. Ltd., New Delhi, India.

Gelucire 44/14, Labrasol ALF and Labrafil M 1944 CS were procured from Gattefossè, Lyon, France. The acetonitrile was obtained from Spectrochem, Mumbai, India. Phospholipid (Phospholipon 90 G) was procured from Lipoid, Ludwigshafen, Germany.

4.2. Methods

4.2.1. Construction of Pseudo-Ternary Phase Diagrams

Series of pseudo-ternary phase diagrams were obtained by the titration method, in which a mixture of oil (isopropyl palmitate) and Smix (surfactant and cosurfactant, i.e., ratios of Gellucire 44/14 and Labrasol) were titrated with water and vice versa. For Smix, three mass ratios of Gellucire 44/14 and Labrasol were prepared in 1:1, 2:1 and 3:1. Various mixtures of water and Smix in the ratios of 1:9, 2:8, 3:7, 4:6, 5:5, 6:4, 7:3, 8:2 and 9:1 were prepared and titrated with oil. For instance, water and S_{mix} were mixed in the weight ratios ranging from 9:1 to 1:9, and every ratio was titrated with oil. During titration, a small volume of oil was added to the mixture and vortexed. Titration was continued until the visual observation of haziness. The volume was noted and all the volumes were converted into mass percentage. Every titration point was plotted on the ternary phase diagram depicting the boundary between the homogeneous and heterogeneous phases. Analogously, various ratios of oil and Smix were prepared and titrated with water until it appeared hazy. The phase diagrams was prepared with the obtained mass percentage data [18,30].

4.2.2. Optimisation of the Microemulsion Composition

From the three developed pseudo-ternary phase diagrams, a total of 9 formulations were prepared, based on the pseudo-ternary phase diagrams. These formulations were coded from F1 to F11. From all the ternary phase diagrams, three oil concentrations were selected, i.e., 12.5%, 15.78% and 22.22%. The composition of the systems is shown in Table 3.

Table 3. Composition of 9 formulation compositions for optimisation.

Formulation Code	F1	F2	F3	F4	F5	F6	F7	F8	F9
Oil (%)	12.5	15.78	22.28	12.5	15.78	22.28	12.5	15.78	22.28
Ternary Phase (S_{mix})	1:1	1:1	1:1	2:1	2:1	2:1	3:1	3:1	3:1
S_{mix} (%)	43.75	42.10	38.88	58.33	56.15	51.85	65.62	63.16	58.33
Water (%)	q.s. to 100	q.s. to 100	q.s. to 100	q.s. to 100	q.s. to 100	q.s. to 100	q.s. to 100	q.s. to 100	q.s. to 100

The amount of mangiferin was kept constant at the concentration of 2% *w/w* in consonance with the previously published reports [31]. These 9 formulations were characterised for various attributes that have been discussed in the subsequent sections. Based on the globule size, various microemulsion parameters and the maximum entrapment efficiency, one formulation was selected for further studies.

4.2.3. Determination of Drug Entrapment Efficiency and Drug Loading

To determine the entrapment efficiency of the developed microemulsion, the dialysis method was employed. In brief, each formulation equivalent to 1 mg of drug was packed in a dialysis bag and sealed. The dialysis bag was suspended in 30.0 mL of methanol and kept for stirring at 50 rpm for 2 h. The dialysis fluid was analysed for the cumulative untrapped drug diffused from the developed system at the end of the study. The drug entrapment efficiency was reported as the amount of entrapped drug per hundred parts of the theoretical drug. On the other hand, the drug loading was reported as the amount of

drug encapsulated per hundred parts of the drug carrier [10,24]. The formulae for the drug entrapment and drug loading were as follows:

$$\text{Drug entrapment efficiency} = \frac{(\text{Total drug} - \text{Diffused Drug})}{\text{Total Drug}} \times 100$$

$$\text{Percent drug loading} = \frac{\text{Entrapped drug}}{\text{Total carrier to entrap the drug}} \times 100$$

4.2.4. Micromeritics, pH, Zeta-Potential and Morphology

The developed formulations were subjected to particle size, particle size distribution and zeta-potential determination using Zetasizer (Nano ZS 90, Malvern, UK). The measurements were recorded in triplicate and the average value was reported as the result. For morphology, transmission electron microscopy was employed using H7000 model (Hitachi Tokyo, Japan). The samples were stained with 1% phosphotungstic acid and placed over carbon-coated copper grid. Systronics pH meter was employed to determine the pH of the undiluted formulations. The pH meter was calibrated with standard buffered solutions over the pH range of 4.0–7.0 and the recordings were made in triplicate, without any dilution.

4.2.5. Fourier Transform Infrared Spectroscopy

The Fourier transform infrared spectroscopy (FT-IR) of various samples were performed on Spectrum 3 FT-IR Spectrometer (PerkinElmer, Waltham, MA, USA). In brief, the samples were punched in potassium bromide pellets and scanned over the wavelength range of 200 cm^{-1} to 4000 cm^{-1} . Liquid samples were adsorbed on the potassium bromide tablets. Interpretations were made using standard reference materials and published reports [32].

4.2.6. Incorporation of the Nanosystem in Hydrogel

Phospholipid (equivalent to 1% *w/w* of the final formulation) was dispersed in water using a magnetic stirrer at 100 rpm to obtain a milky dispersion. A stock of 10% *w/w* Carbopol 934 was prepared in water-dispersed phospholipid and stored overnight. An equal amount of triethanolamine was added drop-wise and the gel was neutralised. The requisite amount of hydrated gel was added in the selected microemulsion, and properly mixed to obtain the desired gel with a Carbopol concentration of 1.25% *w/w* [26]. For the preparation of the conventional gel, mangiferin (2% *w/w*) was dispersed in ethanol (1.25% *w/w*) and Carbopol gel was incorporated by mixing. The swollen gel was neutralised with triethanolamine (1.25% *w/w*) and the final Carbopol content was 1.25 % *w/w*.

4.2.7. Rheology of the Nano-Hydrogel

The developed nano-hydrogel was characterised for the rheological attributes using a Paar Physica cub and bob rheometer at $37 \text{ }^\circ\text{C}$. On average, 5 g of the developed gel was placed in the cup of the rheometer and allowed to equilibrate. The shear stress studied range was 0.1–100 per second and was automatically increased by the software of the equipment, after dipping the bob into the cup. The recordings of the respective shear stress at a particular shear rate were employed for the construction and interpretation of a rheogram. From the rheogram, parameters such as the average viscosity and yield value were determined [33].

4.2.8. Ex Vivo Drug Permeation and Drug Retention Studies

For the ex vivo skin permeation studies and drug retention studies, the excised skins of healthy Laca mice were employed. The methodology and execution of the skin permeation studies and dermatokinetics on rodent skin were duly approved by the Standing Committee of Bioethics Research, Prince Sattam bin Abdulaziz University Al-Kharj, Saudi Arabia, (SCBR-024-2022). To excise the skin, the rodents were sacrificed by cervical dislocation

and the skin was harvested. After the removal of the hair using depilatory cream, the skin was washed thrice with normal saline. The hairless skin was mounted over the donor compartment of the Franz diffusion cell and placed in such a way that its inner side touched the diffusion medium of the receptor compartment. The diffusion medium employed was 30 mL of phosphate-buffered saline of pH 6.8 containing 1% of Tween 80. Plain mangiferin in Carbopol gel (conventional gel), microemulsion and the developed nano-hydrogel were applied on the upper side of the mouse skin in triplicate and the samples from the donor compartment were withdrawn at predetermined time-points. To maintain the sink volume, an equal volume of diffusion medium was replenished after each sample. After filtration, the samples were analysed by HPLC as reported by Allaw et al. [34]. The drug permeation was determined by dividing the amount of drug permeated by the total amount and multiplying it by 100. After the completion of the skin permeation studies, the skin from the donor compartments was removed and washed thrice with water to remove any traces of adhered formulation. The skin was excised into small pieces and placed in measured amount of ethanol overnight for the complete extraction of the drug. After filtration, the amount of drug retained in the skin was determined using HPLC [34,35]. The developed system offered a controlled release pattern following the Fickian drug release and governed by the following equation:

$$j = D \frac{(C_d^0 - C_a)}{X}$$

In the above equation, j is the flux of the drug, C_d^0 is the freely dissolved untrapped drug concentration outside the developed system in the donor compartment, C_a is the acceptor drug concentration, X is the thickness constant and D is the diffusion coefficient.

4.2.9. Cancer Cell Viability Assay and Normal Cell Safety

The in vitro anticancer activity of the developed system and the plain drug was evaluated on MCF-7 breast cancer cell lines. The cells were cultured in 96-welled plates for 48 h with a supply of 5% carbon dioxide. The cells were treated with various concentrations of the formulations and the conventional gel and incubated for 24 h. To each well, 20 μ L of MTT (5 mg/mL) was instilled and incubated for 4 h. In each well, 200 μ L of dimethyl sulfoxide was added to dissolve the formazan crystals. The absorbance values were recorded at 560 nm [10].

4.2.10. Dermal Pharmacokinetic Studies

The dermatokinetic studies were performed analogous to the skin permeation studies, except that, for each time point, one Franz cell was employed. The method reported by Raza et al. was slightly modified [36,37]. The dermis and epidermis were not separated in the present study, but the whole skin was used. It was extracted in ethanol and the drug contents were analysed for that very time point. Analogously, the skin for every time point was processed. The drug amounts for each time point were subjected to one compartment open-body model and various vital dermatokinetic parameters such as first-order permeation rate constant (K_p), the first-order elimination rate constant (K_e), area under the curve (AUC), maximum achievable concentration (C_{max}) and the time required to reach C_{max} (T_{max}) were determined.

Author Contributions: Conceptualisation, A.A. and F.K.A.; methodology, H.S.Y. and A.A.; software, H.S.Y.; validation, A.I.F. and F.K.A.; formal analysis, A.A. and F.K.A.; investigation, A.A. and H.S.Y.; resources, A.I.F.; data curation, F.K.A.; writing—original draft preparation, A.A.; writing—review and editing, F.K.A., A.I.F. and H.S.Y.; visualisation, A.I.F.; supervision, A.A. and H.S.Y.; project administration, A.A. and F.K.A.; funding acquisition, F.K.A. and A.I.F. All authors have read and agreed to the published version of the manuscript.

Funding: This study was supported by funding from Prince Sattam bin Abdulaziz University via project number (PSAU/2023/R/1444).

Institutional Review Board Statement: This study was approved by the Standing Committee on Bioethical Research (SCBR), College of Pharmacy, Prince Sattam Bin Abdulaziz College, Saudi Arabia (research approval number SCBR-024-2022).

Informed Consent Statement: Not applicable.

Data Availability Statement: Not applicable.

Conflicts of Interest: The authors declare no conflict of interest.

References

1. Akter, S.; Moni, A.; Faisal, G.M.; Uddin, M.R.; Jahan, N.; Hannan, A.; Rahman, A.; Uddin, J. Renoprotective Effects of Mangiferin: Pharmacological Advances and Future Perspectives. *Int. J. Environ. Res. Public Health* **2022**, *19*, 1864. [[CrossRef](#)]
2. Wang, M.; Liang, Y.; Chen, K.; Wang, M.; Long, X.; Liu, H.; Sun, Y.; He, B. The management of diabetes mellitus by mangiferin: Advances and prospects. *Nanoscale* **2022**, *14*, 2119–2135. [[CrossRef](#)] [[PubMed](#)]
3. Yap, K.M.; Sekar, M.; Seow, L.J.; Gan, S.H.; Bonam, S.R.; Rani, N.N.I.M.; Lum, P.T.; Subramaniyan, V.; Wu, Y.S.; Fuloria, N.K.; et al. Mangifera indica (Mango): A Promising Medicinal Plant for Breast Cancer Therapy and Understanding Its Potential Mechanisms of Action. *Breast Cancer Targets Ther.* **2021**, *13*, 471–503. [[CrossRef](#)] [[PubMed](#)]
4. Imran, M.; Arshad, M.S.; Butt, M.S.; Kwon, J.-H.; Arshad, M.U.; Sultan, M.T. Mangiferin: A natural miracle bioactive compound against lifestyle related disorders. *Lipids Health Dis.* **2017**, *16*, 1–17. [[CrossRef](#)] [[PubMed](#)]
5. Alam, A.; Alqarni, M.H.; Foudah, A.I.; Raish, M.; Salkini, M.A. Babchi Oil-Based Nanoemulsion Hydrogel for the Management of Psoriasis: A Novel Energy Economic Approach Employing Biosurfactants. *Gels* **2022**, *8*, 761. [[CrossRef](#)]
6. Alam, A.; Foudah, A.I.; Alqarni, M.H.; Yusufoglu, H.S. Microwave-assisted and chemically tailored chlorogenic acid-functionalized silver nanoparticles of Citrus sinensis in gel matrix aiding QbD design for the treatment of acne. *J. Cosmet. Dermatol.* **2023**. [[CrossRef](#)]
7. Singh, R.S.P.; Paul, R.K.; Raza, K.; Mukker, J.K. Pharmacokinetics and pharmacodynamics of nanopharmaceuticals. In *Multifunctional Nanocarriers*; Elsevier: Amsterdam, The Netherlands, 2022; pp. 443–459. [[CrossRef](#)]
8. Paul, R.K.; Kesharwani, P.; Raza, K. Recent update on nano-phytopharmaceuticals in the management of diabetes. *J. Biomater. Sci. Polym. Ed.* **2021**, *32*, 2046–2068. [[CrossRef](#)]
9. Liu, M.; Liu, Y.; Ge, Y.; Zhong, Z.; Wang, Z.; Wu, T.; Zhao, X.; Zu, Y. Solubility, Antioxidation, and Oral Bioavailability Improvement of Mangiferin Microparticles Prepared Using the Supercritical Antisolvent Method. *Pharmaceutics* **2020**, *12*, 90. [[CrossRef](#)]
10. Harsha, P.; Thotakura, N.; Kumar, M.; Sharma, S.; Mittal, A.; Khurana, R.K.; Singh, B.; Negi, P.; Raza, K. A novel PEGylated carbon nanotube conjugated mangiferin: An explorative nanomedicine for brain cancer cells. *J. Drug Deliv. Sci. Technol.* **2019**, *53*, 101186. [[CrossRef](#)]
11. Zhu, Y.; Ye, J.; Zhang, Q. Self-emulsifying Drug Delivery System Improve Oral Bioavailability: Role of Excipients and Physico-chemical Characterization. *Pharm. Nanotechnol.* **2020**, *8*, 290–301. [[CrossRef](#)]
12. Mao, X.; Liu, L.; Cheng, L.; Cheng, R.; Zhang, L.; Deng, L.; Sun, X.; Zhang, Y.; Sarmiento, B.; Cui, W. Adhesive nanoparticles with inflammation regulation for promoting skin flap regeneration. *J. Control. Release* **2019**, *297*, 91–101. [[CrossRef](#)] [[PubMed](#)]
13. Mao, X.; Cheng, R.; Zhang, H.; Bae, J.; Cheng, L.; Zhang, L.; Deng, L.; Cui, W.; Zhang, Y.; Santos, H.A.; et al. Self-Healing and Injectable Hydrogel for Matching Skin Flap Regeneration. *Adv. Sci.* **2018**, *6*, 1801555. [[CrossRef](#)] [[PubMed](#)]
14. Khurana, R.K.; Gaspar, B.L.; Welsby, G.; Katare, O.P.; Singh, K.K.; Singh, B. Improving the biopharmaceutical attributes of mangiferin using vitamin E-TPGS co-loaded self-assembled phospholipidic nano-mixed micellar systems. *Drug Deliv. Transl. Res.* **2018**, *8*, 617–632. [[CrossRef](#)] [[PubMed](#)]
15. Santonocito, D.; Vivero-Lopez, M.; Lauro, M.R.; Torrisi, C.; Castelli, F.; Sarpietro, M.G.; Puglia, C. Design of Nanotechnological Carriers for Ocular Delivery of Mangiferin: Preformulation Study. *Molecules* **2022**, *27*, 1328. [[CrossRef](#)]
16. Katare, O.P.; Raza, K.; Singh, B.; Dogra, S. Novel drug delivery systems in topical treatment of psoriasis: Rigors and vigors. *Indian J. Dermatol. Venereol. Leprol.* **2010**, *76*, 612–621. [[CrossRef](#)]
17. Raza, K.; Kumar, M.; Kumar, P.; Malik, R.; Sharma, G.; Kaur, M.; Katare, O.P. Topical Delivery of Aceclofenac: Challenges and Promises of Novel Drug Delivery Systems. *BioMed Res. Int.* **2014**, *2014*, 406731. [[CrossRef](#)]
18. Raza, K.; Negi, P.; Takyar, S.; Shukla, A.; Amarji, B.; Katare, O.P. Novel dithranol phospholipid microemulsion for topical application: Development, characterization and percutaneous absorption studies. *J. Microencapsul.* **2011**, *28*, 190–199. [[CrossRef](#)]
19. Patel, M.R.; Patel, R.; Parikh, J.R.; Patel, B.G. Novel isotretinoin microemulsion-based gel for targeted topical therapy of acne: Formulation consideration, skin retention and skin irritation studies. *Appl. Nanosci.* **2015**, *6*, 539–553. [[CrossRef](#)]
20. Pleguezuelos-Villa, M.; Nacher, A.; Hernández, M.J.; Buso, M.O.V.; Sauri, A.R.; Díez-Sales, O. Mangiferin nanoemulsions in treatment of inflammatory disorders and skin regeneration. *Int. J. Pharm.* **2019**, *564*, 299–307. [[CrossRef](#)]
21. Negi, J.S. Nanolipid Materials for Drug Delivery Systems: A Comprehensive Review. In *Characterization and Biology of Nanomaterials for Drug Delivery*; Elsevier: Amsterdam, The Netherlands, 2019; pp. 137–163. [[CrossRef](#)]
22. Panigrahi, K.C.; Patra, C.N.; Jena, G.K.; Ghose, D.; Jena, J.; Panda, S.K.; Sahu, M. Gelucire: A versatile polymer for modified release drug delivery system. *Futur. J. Pharm. Sci.* **2018**, *4*, 102–108. [[CrossRef](#)]

23. Hsu, C.-Y.; Wang, P.-W.; Alalaiwe, A.; Lin, Z.-C.; Fang, J.-Y. Use of Lipid Nanocarriers to Improve Oral Delivery of Vitamins. *Nutrients* **2019**, *11*, 68. [[CrossRef](#)] [[PubMed](#)]
24. Jianxian, C.; Saleem, K.; Ijaz, M.; Ur-Rehman, M.; Murtaza, G.; Asim, M.H. Development and in vitro Evaluation of Gastro-protective Aceclofenac-loaded Self-emulsifying Drug Delivery System. *Int. J. Nanomed.* **2020**, *15*, 5217–5226. [[CrossRef](#)] [[PubMed](#)]
25. Lukić, M.; Pantelić, I.; Savić, S. Towards Optimal pH of the Skin and Topical Formulations: From the Current State of the Art to Tailored Products. *Cosmetics* **2021**, *8*, 69. [[CrossRef](#)]
26. Raza, K.; Singh, B.; Singal, P.; Wadhwa, S.; Katare, O.P. Systematically optimized biocompatible isotretinoin-loaded solid lipid nanoparticles (SLNs) for topical treatment of acne. *Colloids Surf. B Biointerfaces* **2013**, *105*, 67–74. [[CrossRef](#)]
27. Negi, P.; Sharma, I.; Hemrajani, C.; Rathore, C.; Bisht, A.; Raza, K.; Katare, O.P. Thymoquinone-loaded lipid vesicles: A promising nanomedicine for psoriasis. *BMC Complement. Altern. Med.* **2019**, *19*, 334. [[CrossRef](#)]
28. Abdullah, A.-S.H.; Mohammed, A.S.; Abdullah, R.; Mirghani, M.E.S.; Al-Qubaisi, M. Cytotoxic effects of *Mangifera indica* L. kernel extract on human breast cancer (MCF-7 and MDA-MB-231 cell lines) and bioactive constituents in the crude extract. *BMC Complement. Altern. Med.* **2014**, *14*, 199. [[CrossRef](#)]
29. Tian, X.; Gao, Y.; Xu, Z.; Lian, S.; Ma, Y.; Guo, X.; Hu, P.; Li, Z.; Huang, C. Pharmacokinetics of mangiferin and its metabolite-Norathyriol, Part 1: Systemic evaluation of hepatic first-pass effect in vitro and in vivo. *Biofactors* **2016**, *42*, 533–544. [[CrossRef](#)]
30. Rao, B.; Vidyadhara, S.; Sasidhar, R.; Chowdhary, Y. Formulation and Evaluation of Liquid Loaded Tablets Containing Docetaxel-Self Nano Emulsifying Drug Delivery Systems. *Trop. J. Pharm. Res.* **2015**, *14*, 567–573. [[CrossRef](#)]
31. Lwin, O.M.; Giribabu, N.; Kilari, E.K.; Salleh, N. Topical administration of mangiferin promotes healing of the wound of streptozotocin-nicotinamide-induced type-2 diabetic male rats. *J. Dermatol. Treat.* **2021**, *32*, 1039–1048. [[CrossRef](#)]
32. Pavia, L.P.; Lampman, G.M.; Kriz, G.S.; James, R.V. *Introduction to Spectroscopy*, 5th ed.; Cengage Publications: Singapore, 2019; pp. 15–106.
33. Raza, K.; Singh, B.; Lohan, S.; Sharma, G.; Negi, P.; Yachha, Y.; Katare, O.P. Nano-lipoidal carriers of tretinoin with enhanced percutaneous absorption, photostability, biocompatibility and anti-psoriatic activity. *Int. J. Pharm.* **2013**, *456*, 65–72. [[CrossRef](#)]
34. Allaw, M.; Pleguezuelos-Villa, M.; Manca, M.L.; Caddeo, C.; Aroffu, M.; Nacher, A.; Diez-Sales, O.; Saurí, A.R.; Ferrer, E.E.; Fadda, A.M.; et al. Innovative strategies to treat skin wounds with mangiferin: Fabrication of transfersomes modified with glycols and mucin. *Nanomedicine* **2020**, *15*, 1671–1685. [[CrossRef](#)]
35. Sharma, G.; Goyal, H.; Thakur, K.; Raza, K.; Katare, O.P. Novel elastic membrane vesicles (EMVs) and ethosomes-mediated effective topical delivery of aceclofenac: A new therapeutic approach for pain and inflammation. *Drug Deliv.* **2016**, *23*, 3135–3145. [[CrossRef](#)] [[PubMed](#)]
36. Raza, K.; Singh, B.; Singla, S.; Wadhwa, S.; Garg, B.; Chhibber, S.; Katare, O.P. Nanocolloidal Carriers of Isotretinoin: Antimicrobial Activity against *Propionibacterium acnes* and Dermatokinetic Modeling. *Mol. Pharm.* **2013**, *10*, 1958–1963. [[CrossRef](#)] [[PubMed](#)]
37. Thotakura, N.; Kumar, P.; Wadhwa, S.; Raza, K.; Katare, P. Dermatokinetics as an Important Tool to Assess the Bioavailability of Drugs by Topical Nanocarriers. *Curr. Drug Metab.* **2017**, *18*, 404–411. [[CrossRef](#)] [[PubMed](#)]

Disclaimer/Publisher's Note: The statements, opinions and data contained in all publications are solely those of the individual author(s) and contributor(s) and not of MDPI and/or the editor(s). MDPI and/or the editor(s) disclaim responsibility for any injury to people or property resulting from any ideas, methods, instructions or products referred to in the content.